PERGAMON

International Journal of Multiphase Flow 26 (2000) 387–419

International Journal of Multiphase Flow

www.elsevier.com/locate/ijmulflow

An experimental and computational study of multiphase flow behavior in a circulating fluidized bed

V. Mathiesen, T. Solberg, B.H. Hjertager*

Telemark Technological R&D Centre (Tel-Tek) and Telemark College (HiT-TF), Kjølnes Ring, N-3914 Porsgrunn, Norway

Received 19 January 1998; received in revised form 12 April 1999

Abstract

This paper presents an experimental and computational study of the flow behavior in a cold flow laboratory scale circulating fluidized bed reactor. Laser Doppler Anemometry and Phase Doppler Anemometry techniques are used to measure mean and fluctuating velocity, diameter and solid concentration, simultaneously. An axial segregation by size and its variation with the superficial gas velocity are demonstrated. Also, a significant radial segregation is measured in the riser. A multi-fluid Computational Fluid Dynamics model has been developed and verified against the experimental results. The flow model is based on an Eulerian description of the phases where the kinetic theory for granular flow forms the basis for the turbulence modeling in the solid phases. The model is generalized for one gas phase and N number of solid phases to enable a realistic description of the particle size distributions in gas/solid flow systems. Each solid phase is characterized by a diameter, form factor, density and restitution coefficient. The computational results agree well with the measurements. © 2000 Elsevier Science Ltd. All rights reserved.

Keywords: LDA/PDA; CFD; Multiphase flow; Circulating fluidized bed; Kinetic theory of granular flow

1. Introduction

The subject of gas/solid flow has for several decades been studied quite extensively, mainly because of its important applications in nuclear, chemical and petroleum industries. Recently, experimental observations of the flow behavior have increased the depth of understanding of

* Corresponding author. Aalborg University Esbjerg, DK-6700, Esbjerg, Denmark.

PII: S0301-9322(99)00027-0

the underlying mechanisms, which in turn has provided the basis for improved field information of the basic conservation equations and constitutive laws for gas/solid flow systems. Although circulating fluidized beds are successfully and widely used in commercial industrial operations, much remains to be done due to the complexity of the gas/solid flow. In order to gain fundamental knowledge about the complex multiphase flow behavior, research is still needed.

To get detailed knowledge about complex gas/solid flow systems, experimental work are obviously important. In this work, Laser Doppler Anemometry (LDA) and Phase Doppler Anemometry (PDA) are used to measure mean and fluctuating velocity, diameter and solid concentration, simultaneously. The different flow behavior of particles of different sizes are studied as well.

Computational fluid dynamics in multiphase flow has become a well accepted and useful tool in modeling of gas/solid flow systems during the recent years, and much progress has been made toward developing computer codes for describing fluidized beds. Most of the developed models are based on a two-phase description, one gas and one solid phase, where all the particles are assumed to be identical, characterized by a diameter, form factor, density and a coefficient of restitution. Most of the models use an Eulerian description of the phases where the constitutive equations of the solid phases are based on the kinetic theory for granular flow with basis of the work of Jenkins and Savage (1983), Lun et al. (1984), Ding and Gidaspow (1990), and Gidaspow (1994). Enwald et al. (1996) and Hjertager (1997) gives a general review of different Eulerian two-phase flow models applied to fluidization.

In gas/solid systems, particle segregation due to different size and/or density will play a significant role on the flow behavior. To describe such phenomena, an extension to multiple particle phases is essential. Jenkins and Mancini (1987) extended the kinetic theory for granular flow to binary mixtures. The basic assumption was equal turbulent kinetic energy with a small correction for the individual phase temperatures. Mathiesen et al. (1996) developed a model based on this work and performed a simulation with one gas and three solid phases. The model predicted segregation effects fairly well, and good agreement with experimental data was obtained.

Gidaspow et al. (1996) and Manger (1996) extended the kinetic theory to binary mixtures of solid with unequal granular temperatures between the phases. Based on their research, a generalized multiphase gas/solid model is given here and the consistency of the model is discussed briefly.

The developed model is used to simulate a cold flow laboratory scale circulating fluidized bed. One gas and two solid phases are used in the simulations. Experimental and computational results are compared and discussed.

2. Experimental measurements technique

During the recent years, LDA has become one of the most commonly used experimental techniques in dilute gas/solid flow systems. The main reasons are that LDA is a non-invasive optical technique which does not disturb the flow, and has a high spatial resolution with a fast

dynamic response and range. LDA together with PDA is able to measure mean and fluctuating velocity, size and concentration of the dispersed phase, simultaneously.

2.1. Particle velocity measurement

When two coherent Gaussian laser beams are intersecting, the intersection will cause a pattern of plane interference fringes. The fringe spacing δ_f can be shown to be proportional to the wavelength λ and inversely proportional to half of the angle ϑ between the two incident beams:

$$\delta_f = \frac{\lambda}{2\sin(\vartheta/2)} \tag{1}$$

When a particle is passing through the intersection area, it will scatter light and the intensity will change according to the interference fringes. The intensity variation of the scattered light or the frequency can be obtained by a photo detector. The velocity of the passing particle will be proportional to the Doppler frequency f_D and the fringe spacing:

$$v_i = f_D \delta_f = \frac{f_D \lambda}{2\sin(\vartheta/2)} \tag{2}$$

where v_i is the absolute velocity of the particle in the direction which is perpendicular to the bisector of the two incident laser beams. To detect the direction of the flow, a frequency shift for one of the beams is introduced. The Doppler frequency is the frequency obtained by the photo detector minus the frequency shift.

The mean velocity, V may be obtained by:

$$V = \frac{1}{N_i} \sum_{i=1}^{N_i} v_i \tag{3}$$

where N_i is the number of sampled particles. The fluctuating velocity or the Root Mean Square (RMS) velocity, V_{RMS} may be expressed as:

$$V_{RMS} = \sqrt{\frac{1}{(N_i - 1)} \sum_{i=1}^{N_i} (v_i - V)^2} \tag{4}$$

2.2. Particle size measurement

Durst and Zare (1975) found that there exists a linear relation between the diameter of a spherical particle and the Doppler signals detected at two different points in space. Almost 10 years later, Saffmann et al. (1984) extended the technique and presented experimental results on bubble size measurements.

The theory is based upon that when two adjacent photo detectors are used to collect scattered laser light, they will show a phase difference which is linearly proportional to the

diameter of a smooth and spherical particle as it passes through the measuring volume (Bachalo and Houser, 1984). The diameter is a function of the phase shift ϕ, the focal length of the transmitting lens f_l, the fringe spacing δ_f, an optical constant K and spacing of the detectors ΔL:

$$D_i = \frac{f_l \delta_f \phi}{360^\circ \Delta L} K \tag{5}$$

The phase difference between two symmetrically placed detectors will be periodic with the particle diameter. Large particles will, therefore, produce a phase difference which is not unique. This ambiguity is removed by adding a third photo detector.

2.3. Particle concentration measurement

The best suitable technique for small particles, sizes less than the measuring volume, is the Time Ratio Technique, Sekoguchi et al. (1982). The technique uses the time ratio of the dispersed phase to the total sampling time to find the average volume fraction of solids. When a particle is in the measuring volume, the local volume fraction ε_i of the dispersed phase may be expressed as:

$$\varepsilon_i = \frac{\pi D_i^3}{6 V_{\text{focus}}} \tag{6}$$

where D_i is the diameter of the ith particle and V_{focus} is the volume of the measuring volume. Within the sampling time period T_{sample}, the average volume fraction of the solid is:

$$\varepsilon_s = \frac{\sum_{i=1}^{N_i} \tau_i \varepsilon_i}{T_{\text{sample}}} \tag{7}$$

The basic assumption of the technique is that there is only one particle in the measuring volume at the same time and, hence, the technique is only suitable for very dilute systems.

3. Multiphase gas/solid model

A multiphase Computational Fluid Dynamics (CFD) model for turbulent gas/solid flow is developed and presented. The model uses an Eulerian description of the phases, and the conservation equations for the solid phases are based on kinetic theory for granular flow with basis on the work of Jenkins and Savage (1983), Lun et al. (1984), Ding and Gidaspow (1990), Gidaspow (1994) and further extended to binary mixtures by Manger (1996). Transport of the distribution functions are described by the Boltzmann equation. The model is modified, generalized and made consistent for one gas phase and N number of solid phases to enable description of realistic particle size distributions. Each solid phase is characterized by diameter, form factor, density and restitution coefficient. The constitutive equations come from the

interactions of the fluctuating and the mean motion of the particles. The interactions give rise to effective shear viscosities, which relates the random motion to the mean motion of the particles. A turbulent kinetic energy equation or granular temperature is derived for each solid phase in order to predict the random fluctuations for each solid phase. The granular temperature is defined as one-third times the fluctuating velocity squared.

To enable modeling of porous plates and obstructions, area and volume porosities are included in the governing equations. The porosities may have values between zero and one, where zero is a totally blocked area/volume and unity is open. This makes it more easy to describe complex geometries such as circulating fluidized beds.

3.1. Transport equations

The CFD model is three-dimensional in Cartesian coordinates, and the governing conservation equations are presented in tensor notation.

3.1.1. Continuity equations

The gas continuity equation is given by:

$$\frac{\partial}{\partial t}\left(\beta_{\mathrm{v}}\varepsilon_{\mathrm{g}}\rho_{\mathrm{g}}\right)+\frac{\partial}{\partial x_i}\left(\beta_i\varepsilon_{\mathrm{g}}\rho_{\mathrm{g}}U_{i,\mathrm{g}}\right)=0 \tag{8}$$

where ε, ρ and U_i are volume fraction, density and the ith direction velocity component, respectively. β_{v} is volume porosity and β_i is the area porosity in ith direction.

The continuity equation for each solid phase is written as:

$$\frac{\partial}{\partial t}\left(\beta_{\mathrm{v}}\varepsilon_{\mathrm{s}}\rho_{\mathrm{s}}\right)+\frac{\partial}{\partial x_i}\left(\beta_i\varepsilon_{\mathrm{s}}\rho_{\mathrm{s}}U_{i,\mathrm{s}}\right)=0 \tag{9}$$

No mass transfer is allowed between the phases.

3.1.2. Momentum equations

The gas phase momentum equation in j-direction may be expressed as:

$$\begin{aligned}&\frac{\partial}{\partial t}\left(\beta_{\mathrm{v}}\varepsilon_{\mathrm{g}}\rho_{\mathrm{g}}U_{j,\mathrm{g}}\right)+\frac{\partial}{\partial x_i}\left(\beta_i\varepsilon_{\mathrm{g}}\rho_{\mathrm{g}}U_{i,\mathrm{g}}U_{j,\mathrm{g}}\right)=\\&\quad-\left(\beta_{\mathrm{v}}\varepsilon_{\mathrm{g}}\right)\frac{\partial P}{\partial x_j}+\frac{\partial}{\partial x_i}\left(\beta_i\tau_{ij,\mathrm{g}}\right)+\beta_{\mathrm{v}}\varepsilon_{\mathrm{g}}\rho_{\mathrm{g}}g_j+\beta_{\mathrm{v}}\sum_{m=1,\ m\neq g}^{M}\Phi_{\mathrm{gm}}\left(U_{j,\mathrm{m}}-U_{j,\mathrm{g}}\right)\end{aligned} \tag{10}$$

P and g_j are fluid pressure and j-direction component of gravity, respectively. Φ_{gm} is drag coefficient between the phases g and m.The stress tensor $\tau_{ij,\mathrm{g}}$ is given by:

$$\tau_{ij,\mathrm{g}}=\mu_{\mathrm{eff,g}}\left[\left(\frac{\partial U_j}{\partial x_i}+\frac{\partial U_i}{\partial x_j}\right)-\frac{2}{3}\delta_{ij}\frac{\partial U_k}{\partial x_k}\right]_{\mathrm{g}} \tag{11}$$

where δ_{ij} is the Kroenecker delta.

The gas phase turbulence is modeled by the Sub Grid Scale (SGS) model proposed by Deardorff (1971), and thus the effective viscosity $\mu_{\mathrm{eff,g}}$ may be estimated as:

$$\begin{aligned}\mu_{\mathrm{eff,g}} &= \varepsilon_{\mathrm{g}}\left(\mu_{\mathrm{lam,g}} + \mu_{\mathrm{turb,g}}\right) = \varepsilon_{\mathrm{g}}\mu_{\mathrm{lam,g}} + \varepsilon_{\mathrm{g}}\rho_{\mathrm{g}}(c_{\mathrm{t}}\Delta)^2\sqrt{S_{ij,\mathrm{g}}:S_{ij,\mathrm{g}}} \\ \Delta &= (\Delta x\Delta y\Delta z)^{1/3} \quad \text{and} \quad S_{ij,\mathrm{g}} = \frac{1}{2}\left[\frac{\partial U_j}{\partial x_i} + \frac{\partial U_i}{\partial x_j}\right]_{\mathrm{g}}\end{aligned} \tag{12}$$

The constant turbulence parameter c_{t} is estimated to be 0.079 by using ReNormalization Group (RNG) theory (Yakhot and Orszag, 1986).

The momentum equations for the solid phases in the j-direction may be written as:

$$\begin{aligned}&\frac{\partial}{\partial t}\left(\beta_{\mathrm{v}}\varepsilon_{\mathrm{s}}\rho_{\mathrm{s}}U_{j,\mathrm{s}}\right) + \frac{\partial}{\partial x_i}\left(\beta_i\varepsilon_{\mathrm{s}}\rho_{\mathrm{s}}U_{i,\mathrm{s}}U_{j,\mathrm{s}}\right) = \\ &\quad -\left(\beta_{\mathrm{v}}\varepsilon_{\mathrm{s}}\right)\frac{\partial P}{\partial x_j} + \frac{\partial}{\partial x_i}\left(\beta_i\Pi_{ij,\mathrm{s}}\right) + \beta_{\mathrm{v}}\varepsilon_{\mathrm{s}}\rho_{\mathrm{s}}g_j + \beta_{\mathrm{v}}\sum_{m=1,\ m\neq s}^{M}\Phi_{\mathrm{sm}}\left(U_{j,\mathrm{m}} - U_{j,\mathrm{s}}\right)\end{aligned} \tag{13}$$

where the total stress tensor $\pi_{ij,\mathrm{s}}$ for each solid phase is:

$$\Pi_{ij,\mathrm{s}} = -P_{\mathrm{s}}\delta_{ij} + \xi_{\mathrm{s}}\delta_{ij}\frac{\partial U_{k,\mathrm{s}}}{\partial x_k} + \mu_{\mathrm{s}}\left[\left(\frac{\partial U_j}{\partial x_i} + \frac{\partial U_i}{\partial x_j}\right) - \frac{2}{3}\delta_{ij}\frac{\partial U_k}{\partial x_k}\right]_{\mathrm{s}} \tag{14}$$

The solid phase pressure P_{s}, bulk viscosity ξ_{s} and shear viscosity μ_{s} are derived from the kinetic theory for granular flow. The solid phase pressure P_{s} consists of a collisional and a kinetic part:

$$P_{\mathrm{s}} = \sum_{n=1}^{N}P_{\mathrm{C,sn}} + \varepsilon_{\mathrm{s}}\rho_{\mathrm{s}}\theta_{\mathrm{s}} \tag{15}$$

where $P_{\mathrm{C,sn}}$ is the pressure caused by collisions between the solid phases s and n, and has the expression:

$$P_{\mathrm{C,sn}} = \frac{\pi}{3}(1+e_{\mathrm{sn}})d_{\mathrm{sn}}^3 g_{\mathrm{sn}}n_{\mathrm{s}}n_{\mathrm{n}}\left\{\frac{m_0\theta_{\mathrm{s}}\theta_{\mathrm{n}}}{\left((m_{\mathrm{s}}/m_{\mathrm{n}})\theta_{\mathrm{s}} + (m_{\mathrm{n}}/m_{\mathrm{s}})\theta_{\mathrm{n}}\right)}\right\}\left\{\frac{(m_0/m_{\mathrm{s}})^2\theta_{\mathrm{s}}\theta_{\mathrm{n}}}{\left(\theta_{\mathrm{s}} + (m_{\mathrm{n}}/m_{\mathrm{s}})^2\theta_{\mathrm{n}}\right)(\theta_{\mathrm{s}}+\theta_{\mathrm{n}})}\right\}^{3/2}$$

$$e_{\mathrm{sn}} = \frac{1}{2}(e_{\mathrm{s}} + e_{\mathrm{n}}), \quad d_{\mathrm{sn}} = \frac{1}{2}(d_{\mathrm{s}} + d_{\mathrm{n}}) \quad \text{and} \quad m_0 = m_{\mathrm{s}} + m_{\mathrm{n}} \tag{16}$$

e, d, n and m are coefficient of restitution, diameter of the particle, number of particles and mass of a particle, respectively. The coefficient of restitution is unity for fully elastic, and zero for inelastic collisions. By using the assumption of spherical particles, number of particles and mass of a particle are, respectively:

$$n_s = \frac{6\varepsilon_s}{\pi d_s^3} \quad \text{and} \quad m_s = \frac{\pi d_s^3 \rho_s}{6} \tag{17}$$

g_{sn} is the radial distribution function, which is nearly one when the flow is dilute and becomes infinite when the flow is so dense that motion is impossible. Based on the single solid phase model given implicitly by Bagnold (1954), a new binary radial distribution function is proposed here:

$$g_0 = \left\{1 - \left(\frac{1-\varepsilon_g}{\varepsilon_{s,max}}\right)^{1/3}\right\}^{-1} \quad g_{sn} = \frac{N}{2}\frac{g_0}{(1-\varepsilon_g)}(\varepsilon_s + \varepsilon_n) \tag{18}$$

where $\varepsilon_{s,max}$ is maximum total volume fraction of solid.

The solid phases bulk viscosity may be written as:

$$\xi_s = \sum_{n=1}^{N} P_{C,sn}\frac{d_{sn}}{3}(\theta_s + (m_n/m_s)\theta_n)\sqrt{\frac{2}{\pi\theta_s\theta_n(\theta_s + (m_n/m_s)^2\theta_n)}} \tag{19}$$

The solid phases shear viscosity consists of a collisional term:

$$\mu_{col,s} = \sum_{n=1}^{N} P_{C,sn}\frac{d_{sn}}{5}(\theta_s + (m_n/m_s)\theta_n)\sqrt{\frac{2}{\pi\theta_s\theta_n(\theta_s + (m_n/m_s)^2\theta_n)}} \tag{20}$$

and a kinetic term:

$$\mu_{kin,s} = \frac{2\mu_{dil,s}}{\frac{1}{N}\sum_{n=1}^{N}(1+e_{sn})g_{sn}}\left\{1 + \frac{4}{5}\sum_{n=1}^{N} g_{sn}\varepsilon_n(1+e_{sn})\right\}^2 \tag{21}$$

where

$$\mu_{dil,s} = \frac{15}{8d_s^3}\varepsilon_s l_s\sqrt{\frac{2m_s\theta_{s,av}}{\pi}} \quad \text{and} \quad l_s = \frac{1}{6\sqrt{2}}\frac{d_s}{\varepsilon_s} \tag{22}$$

To ensure that the dilute viscosity is finite as the volume fraction of solid approaches zero, the mean free path l_s is limited by a characteristic dimension. The average granular temperature $\theta_{s,av}$ is obtained from:

$$\theta_{s,av} = \frac{2m_s\theta_s}{\left\{\sum_{n=1}^{N}\left(\frac{n_n}{n_s}\right)\left(\frac{d_{sn}}{d_s}\right)^2\sqrt{\frac{(m_0/m_s)^2\theta_n}{(\theta_s + (m_n/m_s)^2)\theta_n}}S^{3/2}\right\}^2} \tag{23}$$

$$S = \frac{(m_0/m_s)^2\theta_s\theta_n}{(\theta_s + (m_n+m_s)^2\theta_n)(\theta_s+\theta_n)}$$

For $\varepsilon_g \leq 0.8$, the gas/solid drag coefficients are based on Ergun equation (Ergun, 1952):

$$\Phi_{sg} = 150\frac{\varepsilon_s(1-\varepsilon_g)\mu_{lam,g}}{\varepsilon_g(\psi_s d_s)^2} + 1.75\frac{\varepsilon_s\rho_g|\vec{u}_g - \vec{u}_s|}{\psi_s d_s} \tag{24}$$

where ψ_s is the form factor which is unity for spheres and between zero and one for all other particles. For $\varepsilon_g > 0.8$, the drag coefficients are based on the work by Wen and Yu (1966), and Rowe (1961):

$$\Phi_{sg} = \frac{3}{4}C_d\frac{\varepsilon_s\varepsilon_g\rho_g|\vec{u}_g - \vec{u}_s|}{\psi_s d_s}\varepsilon_g^{-2.65}$$

$$C_d = \begin{cases} \dfrac{24}{Re_s}\left(1 + 0.15Re^{0.687}\right) & \text{for } Re_s \leq 1000 \\ 0.44 & \text{for } Re_s > 1000 \end{cases} \tag{25}$$

$$Re_s = \frac{d_s\rho_g\varepsilon_g|\vec{u}_g - \vec{u}_s|}{\mu_{lam,g}}$$

The particle/particle drag coefficients may be expressed as (Manger, 1996):

$$\Phi_{sn} = P_{C,sn}\left\{\frac{3}{d_{sn}}\sqrt{\frac{2(m_s^2\theta_s + m_n^2\theta_n)}{\pi m_0^2\theta_s\theta_n}} + \frac{1}{|\vec{u}_n - \vec{u}_s|}\left[\nabla|\ln\frac{\alpha_s}{\alpha_n}| + \frac{\theta_s\theta_n}{\theta_s + \theta_n}|\frac{\nabla\theta_n}{\theta_n^2} - \frac{\nabla\theta_s}{\theta_s^2}| + 3\nabla|\frac{\ln(m_n\theta_n)}{\ln(m_s\theta_s)}|\right]\right\} \tag{26}$$

3.1.3. Turbulent kinetic energy equations

A transport equation for turbulent kinetic energy or granular temperature equation is defined for each solid phase, i.e.:

$$\frac{3}{2}\left[\frac{\partial}{\partial t}(\beta_v\varepsilon_s\rho_s\theta_s) + \frac{\partial}{\partial x_i}(\beta_i\varepsilon_s\rho_s U_{i,s}\theta_s)\right] = \beta_v\left(\Pi_{ij,s}:\frac{\partial U_{j,s}}{\partial x_i}\right) + \frac{\partial}{\partial x_i}\left(\beta_i\kappa_s\frac{\partial\theta_s}{\partial x_i}\right) - \beta_v\gamma_s - 3\beta_v\Phi_{sg}\theta_s \tag{27}$$

Here, the terms on the right side of the equation represent production due to shear, diffusive transport, dissipation due to inelastic collisions and dissipation due to fluid friction. A production term due to fluctuations in drag has been assumed as negligible. This is a reasonable assumption for the relatively large and heavy glass particles considered in this work.

Hence, the particle response time is assumed to be much longer than the characteristic time scale for the turbulent fluid motion.

The conductivity of granular temperature κ_s, and the dissipation due to inelastic collisions γ_s are determined from the kinetic theory for granular flow. The conductivity is given by a dilute and a dense part as:

$$\kappa_s = \frac{2\kappa_{dil,s}}{\frac{1}{N}\sum_{n=1}^{N}(1+e_{sn})g_{sn}}\left\{1+\frac{6}{5}\sum_{n=1}^{N}g_{sn}\varepsilon_n(1+e_{sn})\right\}^2 + 2\varepsilon_s\rho_s d_s\sqrt{\frac{\theta_s}{\pi}}\sum_{n=1}^{N}\varepsilon_n g_{sn}(1+e_{sn})$$

$$\kappa_{dil,s} = \frac{225}{32}\varepsilon_s l_s\sqrt{\frac{2m_s\theta_{s,av}}{\pi}} \tag{28}$$

The collisional dissipation is given by:

$$\gamma_s = \sum_{n=1}^{N}\frac{3}{4}P_{C,sn}\frac{(1-e_{sn})}{d_{sn}}\left[4\sqrt{\frac{2\theta_s\theta_n}{\pi\left((m_s/m_0)^2\theta_s+(m_n/m_0)^2\theta_n\right)}}\right.$$

$$\left. - d_{sn}\left(\frac{(m_s/m_0)\theta_s+(m_n/m_0)\theta_n}{(m_s/m_0)^2\theta_s+(m_n/m_0)^2\theta_n}\right)\frac{\partial U_{k,s}}{\partial x_k}\right] \tag{29}$$

3.2. Consistency of the multiphase model

A multiphase gas/solid flow model based on kinetic theory for granular flow has been presented. In order to handle realistic particle distributions, the multiphase model has been extended from a single solid phase to multiple solid phases. Before the multiphase gas/solid flow model is applied, the generalization from a single solid phase to multiple solid phases is demonstrated to be consistent.

There are two requirements for model consistency that must be fulfilled. The first requirement is that the multiphase gas/solid flow model with multiple solid phases must reduce to the corresponding model with a single solid phase, if the number of solid phases are chosen equal to one. The second requirement is that a solid phase consisting of particles with identical diameter, density and coefficient of restitution can be represented either as a single solid phase of volume fraction ε_s or as N distinct solid phases, whose respective volume fractions will sum to ε_s.

3.2.1. Single solid phase

For a single solid phase, the momentum equation and the constitutive equations presented by Eqs. (13)–(26) will be reduced to following equations:

$$\frac{\partial}{\partial t}\left(\beta_{\mathrm{v}}\varepsilon_{\mathrm{s}}\rho_{\mathrm{s}}U_{j,\mathrm{s}}\right)+\frac{\partial}{\partial x_i}\left(\beta_i\varepsilon_{\mathrm{s}}\rho_{\mathrm{s}}U_{i,\mathrm{s}}U_{j,\mathrm{s}}\right)$$

$$=-\left(\beta_{\mathrm{v}}\varepsilon_{\mathrm{s}}\right)\frac{\partial P}{\partial x_j}+\frac{\partial}{\partial x_i}\left(\beta_i\Pi_{ij,\mathrm{s}}\right)+\beta_{\mathrm{v}}\varepsilon_{\mathrm{s}}\rho_{\mathrm{s}}g_j+\Phi_{\mathrm{sg}}\left(U_{j,\mathrm{g}}-U_{j,\mathrm{s}}\right) \tag{30}$$

The total stress tensor for the single solid phase model is identically to Eq. (14), but the solid phase pressure will be simplified to:

$$P_{\mathrm{s}}=\varepsilon_{\mathrm{s}}\rho_{\mathrm{s}}\left(1+2(1+e_{\mathrm{s}})\varepsilon_{\mathrm{s}}g_0\right)\theta_{\mathrm{s}} \tag{31}$$

The single solid phase bulk viscosity can be written as:

$$\xi_{\mathrm{s}}=\frac{4}{3}\varepsilon_{\mathrm{s}}^2\rho_{\mathrm{s}}d_{\mathrm{s}}g_0(1+e_{\mathrm{s}})\sqrt{\frac{\theta_{\mathrm{s}}}{\pi}} \tag{32}$$

The solid phase shear viscosity may be rewritten as:

$$\mu_{\mathrm{s}}=2\frac{\mu_{\mathrm{dil,s}}}{(1+e_{\mathrm{s}})g_0}\left(1+\frac{4}{5}(1+e_{\mathrm{s}})g_0\varepsilon_{\mathrm{s}}\right)^2+\frac{4}{5}\varepsilon_{\mathrm{s}}^2\rho_{\mathrm{s}}d_{\mathrm{s}}g_0(1+e_{\mathrm{s}})\sqrt{\frac{\theta_{\mathrm{s}}}{\pi}} \tag{33}$$

where

$$\mu_{\mathrm{dil,s}}=\frac{5}{16}\rho_{\mathrm{s}}\varepsilon_{\mathrm{s}}l_{\mathrm{s}}\sqrt{2\pi\theta_{\mathrm{s}}}\quad\text{and}\quad l_{\mathrm{s}}=\frac{1}{6\sqrt{2}}\frac{d_{\mathrm{s}}}{\varepsilon_{\mathrm{s}}} \tag{34}$$

The transport equation for the turbulent kinetic energy of a single solid phase is equivalent to Eq. (27). The transport coefficient is reduced to:

$$\kappa_{\mathrm{n}}=\frac{2\kappa_{\mathrm{dil,s}}}{(1+e_{\mathrm{s}})g_0}\left(1+\frac{6}{5}(1+e_{\mathrm{s}})g_0\varepsilon_{\mathrm{s}}\right)^2+2\varepsilon_{\mathrm{s}}^2\rho_{\mathrm{s}}d_{\mathrm{s}}g_0(1+e_{\mathrm{s}})\sqrt{\frac{\theta_{\mathrm{s}}}{\pi}} \tag{35}$$

where

$$\kappa_{\mathrm{dil,s}}=\frac{75}{64}\rho_{\mathrm{s}}\varepsilon_{\mathrm{s}}l_{\mathrm{s}}\sqrt{2\pi\theta_{\mathrm{s}}}\quad\text{and}\quad l_{\mathrm{s}}=\frac{1}{6\sqrt{2}}\frac{d_{\mathrm{s}}}{\varepsilon_{\mathrm{s}}} \tag{36}$$

The collisional energy dissipation is simplified to:

$$\gamma_{\mathrm{s}}=3\left(1-e_{\mathrm{s}}^2\right)\varepsilon_{\mathrm{s}}^2\rho_{\mathrm{s}}g_0\theta_{\mathrm{s}}\left(\frac{4}{d_{\mathrm{s}}}\sqrt{\frac{\theta_{\mathrm{s}}}{\pi}}-\frac{\partial U_{k,\mathrm{s}}}{\partial x_k}\right) \tag{37}$$

The model presented by Eqs. (30)–(37) is the same as the single solid phase model proposed by Gidaspow (1994). This model is also the starting point for the present multiphase gas/solid flow model with multiple solid phases.

3.2.2. Two identical solid phases

If a gas/solid system is modeled by N solid phases with particles of identical diameter, form

factor, density and coefficients of restitution, the mathematical model for a single solid phase described by Eqs. (30)–(37) should be retained. For simplicity, the number of identical solid phases N is chosen to be 2, and, therefore:

$$\varepsilon_s = \varepsilon_1 + \varepsilon_2 \tag{38}$$

By adding the momentum equations for the solid phases 1 and 2, a common momentum balance for the solid phases may be obtained:

$$\begin{aligned}
&\frac{\partial}{\partial t}\left(\beta_v \varepsilon_s \rho_s U_{j,s}\right) + \frac{\partial}{\partial x_i}\left(\beta_i \varepsilon_s \rho_s U_{i,s} U_{j,s}\right) = -\left(\beta_v \varepsilon_s\right)\frac{\partial P}{\partial x_j} \\
&+\frac{\partial}{\partial x_i}\left[\beta_i\left((P_1+P_2)\delta_{ij} + (\xi_1+\xi_2)\delta_{ij}\frac{\partial U_{k,s}}{\partial x_k} + (\mu_1+\mu_2)\left(\frac{\partial U_j}{\partial x_i} + \frac{\partial U_i}{\partial x_i} - \frac{2}{3}\delta_{ij}\frac{\partial U_k}{\partial x_k}\right)_s\right)\right] \\
&+\beta_v \varepsilon_s \rho_s g_j + \left(\Phi_{1g} + \Phi_{2g}\right)\left(U_{j,g} - U_{j,s}\right)
\end{aligned} \tag{39}$$

The momentum Eqs. (30) and (39) are identical, if the following equalities are satisfied:

$$\begin{aligned}
P_s &= P_1 + P_2 \\
\xi_s &= \xi_1 + \xi_2 \\
\mu_s &= \mu_1 + \mu_2 \\
\Phi_{sg} &= \Phi_{1g} + \Phi_{2g}
\end{aligned} \tag{40}$$

Likewise, the transport equations for the turbulent kinetic energy or granular temperature in the two formulations can be shown to be identical, if the following equalities are satisfied:

$$\begin{aligned}
\kappa_s &= \kappa_1 + \kappa_2 \\
\gamma_s &= \gamma_1 + \gamma_2
\end{aligned} \tag{41}$$

The equalities in Eqs. (40) and (41) can be shown to be fulfilled, if the collisional pressures satisfy the following relation:

$$P_{C,s} = P_{C,1} + P_{C,2} \tag{42}$$

The collisional pressure for a single solid phase is given by:

$$P_{C,s} = 2(1+e_s)\varepsilon_s^2 \rho_s g_0 \theta_s \tag{43}$$

For two identical solid phases, the sum of the collisional pressures are:

$$P_{C,1} + P_{C,2} = 2(1+e_s)\varepsilon_1^2 \rho_s g_{11}\theta_s + 2(1+e_s)2\varepsilon_1\varepsilon_2\rho_s g_{12}\theta_s + 2(1+e_s)2\varepsilon_2^2\rho_s g_{22}\theta_s \tag{44}$$

Comparing Eqs. (43) and (44) leads to:

$$\varepsilon_s^2 g_0 = \varepsilon_1^2 g_{11} + 2\varepsilon_1\varepsilon_2 g_{12} + \varepsilon_2^2 g_{22} \tag{45}$$

For the multiphase gas/solid models with either a single solid phase or multiple identical solid phases to be the same, the almost trivial finding is reached that the radial distribution function must be the same, i.e.,

$$g_0 = g_{11} = g_{12} = g_{22} \tag{46}$$

Deriving binary radial distribution functions, which behave properly, is clearly not straightforward. In the literature, Lebowitz (1964), Jenkins and Mancini (1987), Zamankhan (1995) and Boemer (1996) have proposed different models for the binary radial distribution function. However, none of these models reduce to the monodispersed radial distribution function for multiple solid phases with identical particles, become infinite for maximum solid packing and are an expression for a probability of collision between two solid phases.

The binary radial distribution function proposed in Eq. (18) satisfy all three requirements, provided that the initial volume fractions for solid phases 1 and 2 are:

$$\varepsilon_1 = \varepsilon_2 = \frac{1}{2}\varepsilon_s \tag{47}$$

It should be noted that the fraction of the phases only have to be initially identical. If they are, the volume fractions of the two solid phases will be equal at each point in time and space, since Eqs. (40) and (41) are satisfied. This shows that a solid phase consisting of particles with identical diameter, density and coefficient of restitution can be represented either as a single solid phase of volume fraction ε_s or as N distinct solid phases, whose respective volume fraction is ε_s/N. Otherwise, when considering N solid phases which are not identical, the concentrations of the solid phases do not have to be equal.

4. Solution procedure

The governing equations are solved by a finite volume method (Patankar, 1980). The calculation domain is divided into a finite number of control volumes. At main grid points placed in the center of the control volume, volume fraction, density and turbulent kinetic energy are stored. A staggered grid arrangement is used and the velocity components are stored at the control volume surfaces. The conservation equations are integrated in space and time. This integration is performed using upwind differencing in space and implicit in time. The set of algebraic equation are solved by the TriDiagonal-Matrix Algorithm, except for the volume fraction where a point iteration method is used. Due to the strong coupling between the phases through the drag forces, the two-phase Partial Elimination Algorithm (PEA) (Spalding, 1985) is generalized to multiple phases, and is used to de-couple the drag. The InterPhase-Slip Algorithm (IPSA) is used to take care of the coupling between continuity and the velocity equations, from Spalding (1983).

5. Experimental setup

An experimental study of a cold flow laboratory scale circulating fluidized bed using LDA and PDA are conducted. In the riser of the circulating fluidized bed, diameter, velocity and volume fraction measurements are performed, simultaneously. The dispersed phase is spherical glass particles which are classified as group B particles (Geldart, 1973). A LDA/PDA system delivered by DANTEC is used in the experimental study. The experiments are conducted with one dilute particle concentration and with three different superficial gas velocities.

5.1. Circulating fluidized bed

The riser has a internal diameter of 0.032 m, is 1.0 m high and made of clear plexiglass. The primary gas inlet is located at the bottom of the riser. To provide a uniform gas velocity at the inlet, an air distributor is installed. The distributor is a filter-plate with a thickness and porosity of 0.004 m and 0.36, respectively.

At the top of the riser, the suspended particles enter a glass cyclone where the solid are separated from the gas and recycled via a return loop. Supply of secondary air, positioned 0.05 m

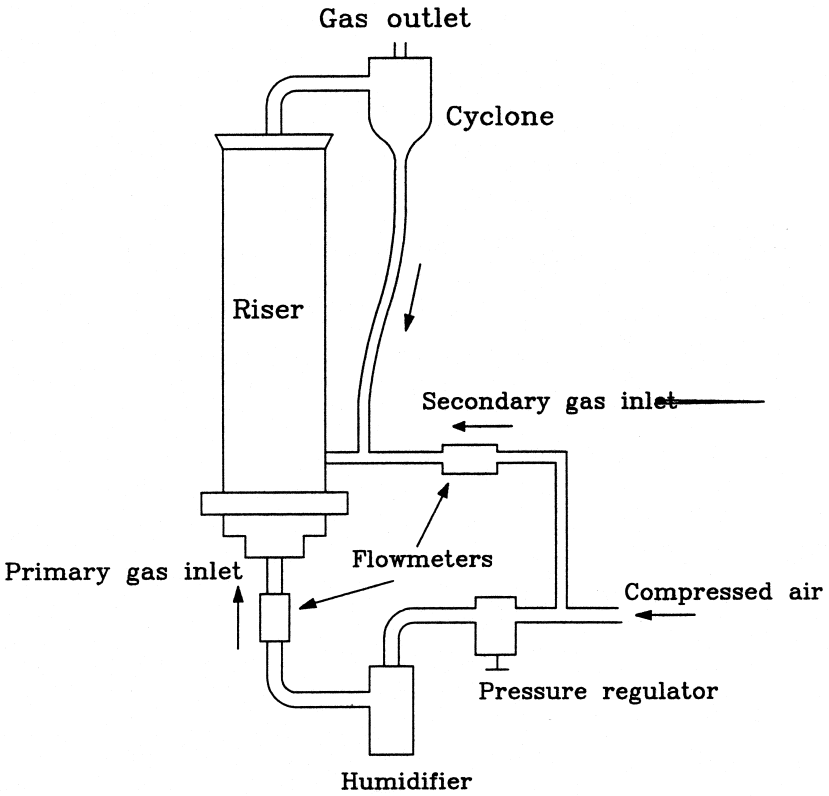

Fig. 1. A schematic sketch of the laboratory scale CFB.

above the air distributor feeds the solid back to the riser. Fig. 1 shows a schematic sketch of the circulating fluidized bed system.

The air has ambient temperature and pressure. To minimize the influence of electrostatic effects, a humidifier is installed upstream the main air inlet.

The measurements are conducted with three different superficial gas velocities, 0.8, 1.0 and 1.2 m/s, respectively. To prevent the particles to build up in the recirculation loop, the secondary air inlet velocity is held constant at 0.3 m/s. The secondary air inlet has a diameter of 0.008 m.

From a Gaussian particle size distribution with a Sauter mean diameter of 157 μm, two distinct particle groups are sieved out. The sieved particles have diameters between 100 and 130 m, and between 175 and 205 m for the smallest and largest particles, respectively. The mean particle diameter of the two groups are approximately 120 and 185 μm. The two distinct particle groups are mixed together and the initial volume concentration of each group is identical. The initial bed height is 0.04 m. Thus, the overall volume concentration of solid in the riser is 2.5%. The particle density is 2400 kg/m^3.

5.2. Laser and phase Doppler anemometry

The laser source is a 2 W Spectra-Physics Stabilite 2016 Argon-Ion laser operating at a wavelength of 514.5 nm. The LDA/PDA system is applied in an off-axis back scatter modus. The transmitting and receiving lenses have focal length of 310 and 600 mm, respectively. Table 1 gives a summary of the most essential LDA/PDA parameters.

The measurements are performed at three heights 0.2, 0.4 and 0.7 m above the main gas inlet, respectively. At each height the measurements are done at 25 different radial positions, from wall to wall. An IBM compatible computer is used on-line for data acquisition and processing. Mean particle velocity and fluctuating velocity profiles are obtained for each particle group. Volume fraction profiles of solid and mean diameter profiles are measured as well. Mean diameters along the center axis are also measured and presented. The local mean diameters and velocities are the mean values of 3000 accepted samples in each measuring point.

Table 1
LDA/PDA parameters

Fringe spacing	4.2 μm
Beam separation	38 mm
Focal length, transmitting lens	310 mm
Focal length, receiving lens	600 mm
Width of measuring volume	0.15 mm
Length of measuring volume	2.45 mm
Effective scattering angle	124°
Velocity range	−1.26 to 3.28 m/s
Particle/gas refraction index	1.51/1.00

6. Numerical parameters, initial and boundary conditions

The whole circulating fluidized bed loop as shown in Fig. 1, is modeled and simulated in a two-dimensional Cartesian coordinate system. The calculation domain is divided into 29 × 102 control volumes in radial and axial direction, respectively. The grid is uniform in the axial direction, but in the radial direction a non-uniform grid is used in order to have smaller control volumes close to the walls, where the volume fraction and velocity gradients increase. Although a grid dependence study is clearly desirable, the long computational times involved make such a study infeasible. Based on previous experiences (e.g., Samuelsberg and Hjertager, 1996a, 1996b), the grid resolution appears, nevertheless, to be adequate. The circulating fluidized bed model with internal obstructions and grid nodes is shown in Fig. 2.

Two solid phases are used to describe the particles. The two solid phases have identical flow parameters, but different particle diameters. Table 2 gives a summary of the flow parameters.

The reactor is initially filled with a 0.04 m high bed, where the total volume fraction of solid is approximately 0.63. The two solid phases are perfectly mixed in the bed and are assumed to have an identical initial volume fraction.

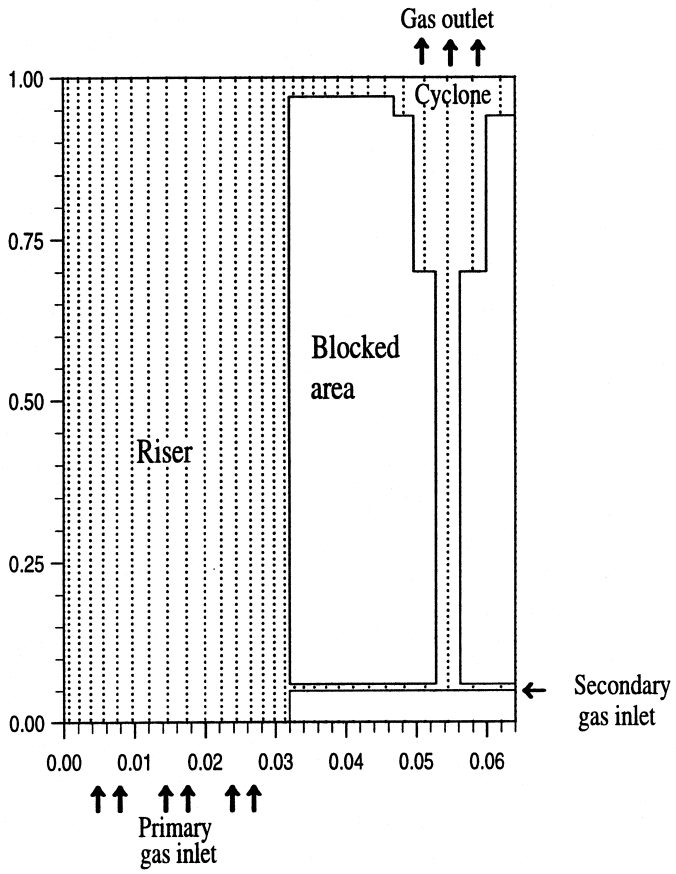

Fig. 2. Calculation domain with internal obstructions and grid nodes.

Table 2
Numerical flow parameters

	Gas phase	Solid phase I	Solid phase II
Mean diameter (μm)	–	120	185
Density (kg/m^3)	1.20	2400	2400
Form factor	–	1.00	1.00
Laminar viscosity (kg/ms)]	1.8E−5	–	–
Restitution coefficient, solid	–	0.99	0.99
Courant number		1.00	
Maximum total volume fraction of solid		0.63	

One-dimensional plug flow is assumed at the primary as well as at the secondary gas inlet. At the outlet, which is located at the top of the cyclone, a continuity condition for the gas phase is used. No particles are allowed to leave the circulating fluidized bed system. At the walls, the no-slip wall condition is used for the gas. Even though a humidifier was installed to prevent electrostatic effects, significant static electricity was observed during the experiments, and particles were sticking to the wall. Due to this a no-slip condition is also used for the solid phases. A zero gradient condition is used for the turbulent kinetic energy.

All the simulations are run for 12 s of real time. The time averaged results are obtained from the last two seconds of the simulations.

7. Experimental and computational results

In the experimental as well as in the computational study, particular emphasis is given to the flow condition with a superficial gas velocity of 1.0 m/s. Flow conditions with lower and higher superficial gas velocity, 0.8 and 1.2 m/s, respectively, are used to investigate the sensitivity and general trends of the flow behavior.

7.1. Particle diameter profiles

The particle size distribution is important in chemical reactors, and axial as well as radial segregation by size will have large influence on the reaction kinetics and catalyst activity. It is well accepted knowledge that risers can generally be divided into three distinct zones. Above the inlet, there will be a section looked upon as a dense turbulent bubbling bed with nearly constant concentration of solid. In this region, the averaged particle size will be large. Above the dense zone comes a freeboard zone with a smaller averaged particle size and a significant decreasing of solid concentration. At the top of the riser an exit zone will exist. Depending on the outlet geometry, the concentration of solid will decrease/increase and the particle diameter

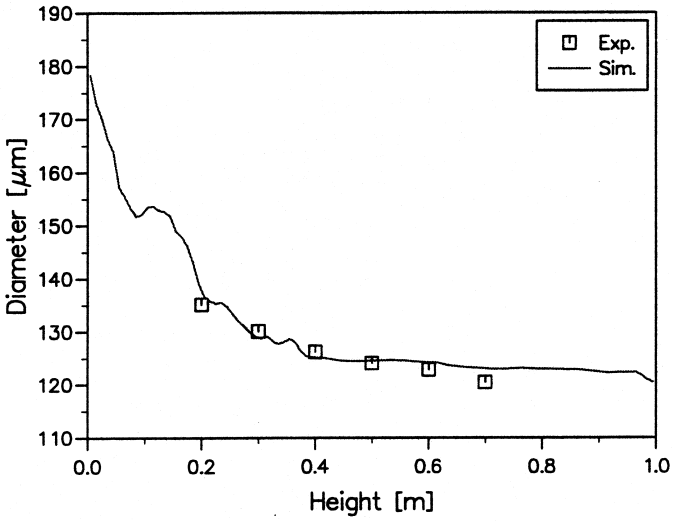

Fig. 3. Axial particle diameter profile, $V_{SUP} = 1.0$ m/s.

will normally be small. When the superficial gas velocity increases, the solid concentration distribution as well as the diameter distribution will be more uniform in the axial direction.

Fig. 3 shows the measured and computed axial number averaged diameter profile along the center axis of the riser. The superficial gas velocity is 1.0 m/s. The averaged diameter is significantly decreasing with the height above the inlet. The measurements show that from 0.2 to 0.7 m above the primary gas inlet, the averaged diameter decreases from 135 to 120 μm. Due to a dense zone, it was not possible to conduct measurements lower than 0.2 m above the inlet. However, the experimentally obtained mean diameter seems to increase exponentially in the dense zone. The simulation shows exactly the same trend and the maximum deviation between measurements and simulation is just about 2 μm.

The experimental and computational results show the importance of using more than one solid phase in modeling of a gas/solid flow system with a non-uniform particle size distribution. With one solid phase, the deviation between the real and actual diameter would have been 30–40 μm in most of the riser. By using two solid phases the maximum deviation is reduced to about 2 μm.

With different superficial gas velocities, the form and slope of the axial diameter profile will be changed. This is shown in Fig. 4. When the gas velocity decreases, the particles are more difficult to fluidize and only the smallest particles will reach the freeboard zone and circulate in the loop. In the dense section, a very large mean diameter is observed. By increasing the gas velocity a more uniform axial diameter distribution appears. The mathematical model predicts the axial segregation very well for all flow conditions and only insignificant deviations from the experimental data are observed.

Core-annulus flow will normally occur in the riser of a circulating fluidized bed and is frequently observed and reported in the literature. Core-annulus flow is characterized by a nearly constant particle upflow and relatively small concentration of solid in the central part of the riser, called the core region. Near the wall, in the annulus, the concentration of solid

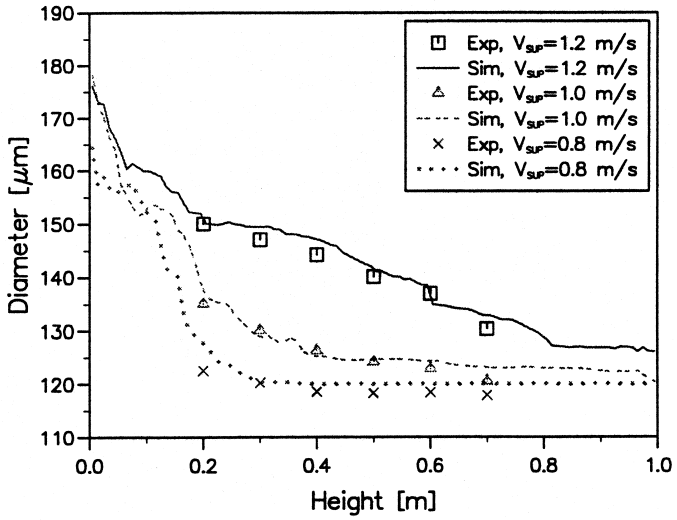

Fig. 4. Axial particle diameter profiles for different superficial gas velocities.

increases and there will be a downflow of solid. No significant radial variation of the particle mean diameter in the annulus and the core regions seems to be observed and reported in earlier studies of fluidized beds.

Fig. 5 shows the measured and computed averaged particle diameter profiles at three different heights, above the inlet. The experimental data does not support the behavior reported in the literature of the subject, and shows a significant difference in the mean diameter at the center of the riser and near the wall. The difference increases with the height above inlet, which means decreasing concentration of solid. The mathematical model predicts a correct mean diameter in the core region at all heights, but is not able to calculate the significant increases of mean diameter in the wall region.

Fig. 6 shows a comparison of the mean particle diameter profiles for different superficial gas velocities, 0.4 m above the main gas inlet. With a gas velocity of 0.8 m/s, the concentration, 0.4 m above the inlet, is very dilute and the radial diameter segregation is large.

By increasing the gas velocity, the concentration increases and the radial diameter variation decreases. This means less radial segregation or more radial mixing. For all simulations, the mean diameter in the central part is in good agreement with the experimental results, although discrepancies are observed in the annulus region.

The axial segregation, due to different particle diameters, is explained by the fact that smaller particles are more easy to fluidize and will follow the gas more effectively than larger ones. From the empirical drag coefficient given in Eq. (19), it can be shown that the minimum fluidization velocity is proportional to the mean diameter. The segregation by size will be reduced when the superficial gas velocity and, hence, gas/solid drag increases. Also, the particle–particle drag, which is proportional to the square root of the turbulent kinetic energy, plays a major role at the segregation by size.

The radial segregation of the mean diameter may be explained by the same phenomena. Larger particles will not follow the gas effectively and start accumulating, particularly in the

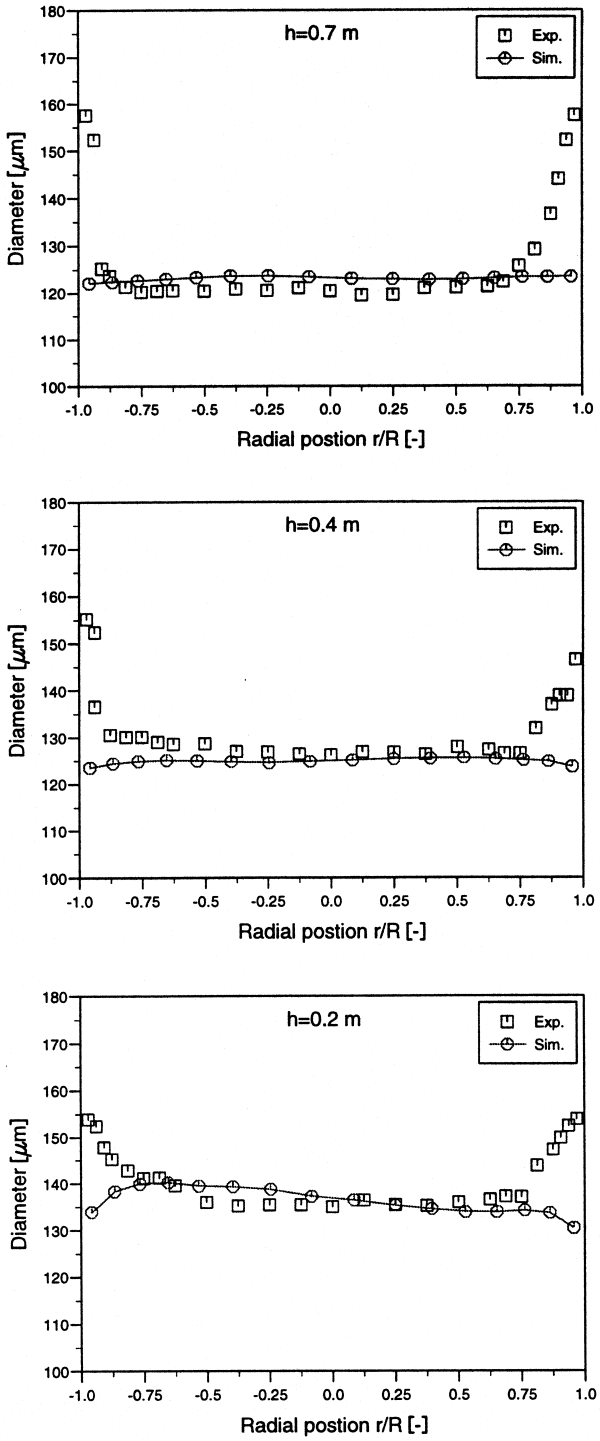

Fig. 5. Mean particle diameter profiles at different heights, $V_{SUP} = 1.0$ m/s.

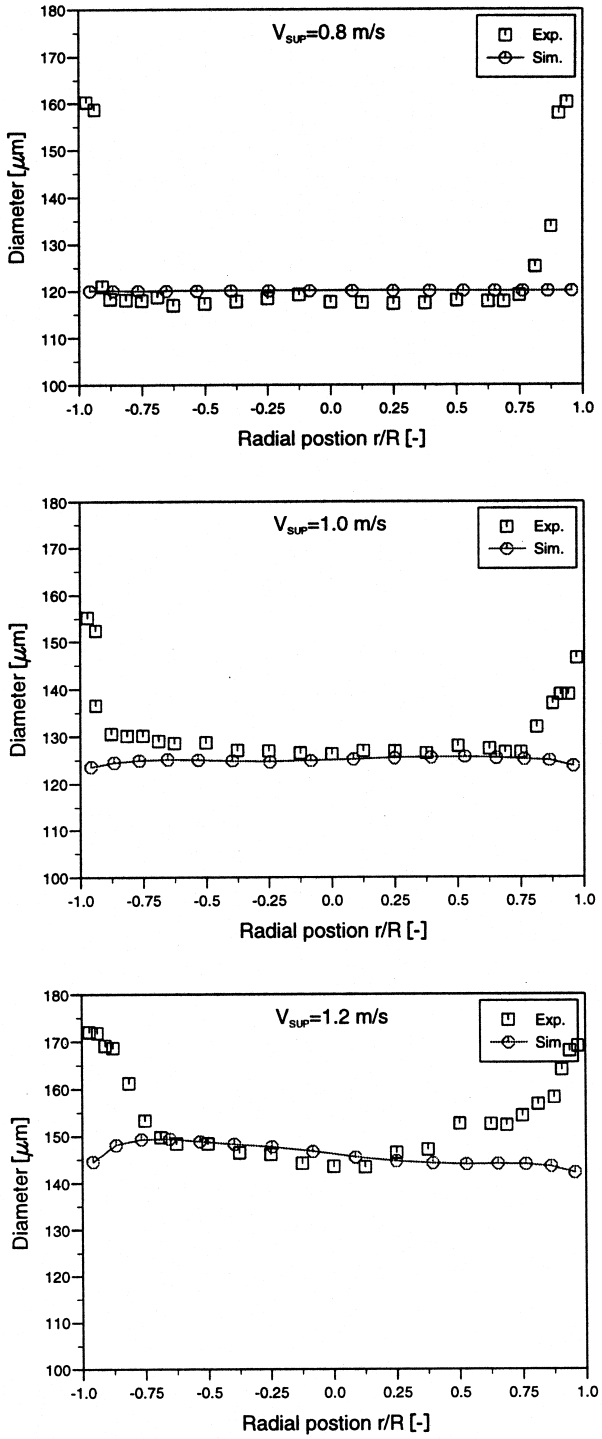

Fig. 6. Mean particle diameter profiles for different superficial gas velocities, $h = 0.4$ m.

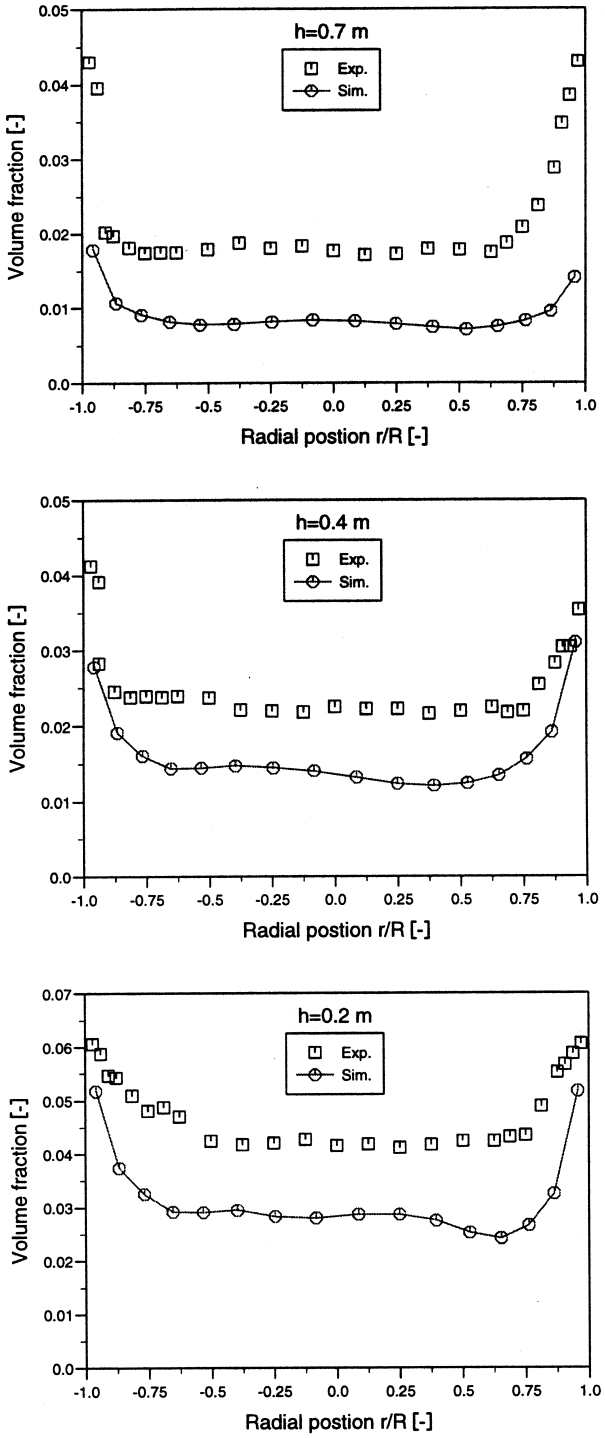

Fig. 7. Volume fraction profiles of solid at different heights, $V_{SUP} = 1.0$ m/s.

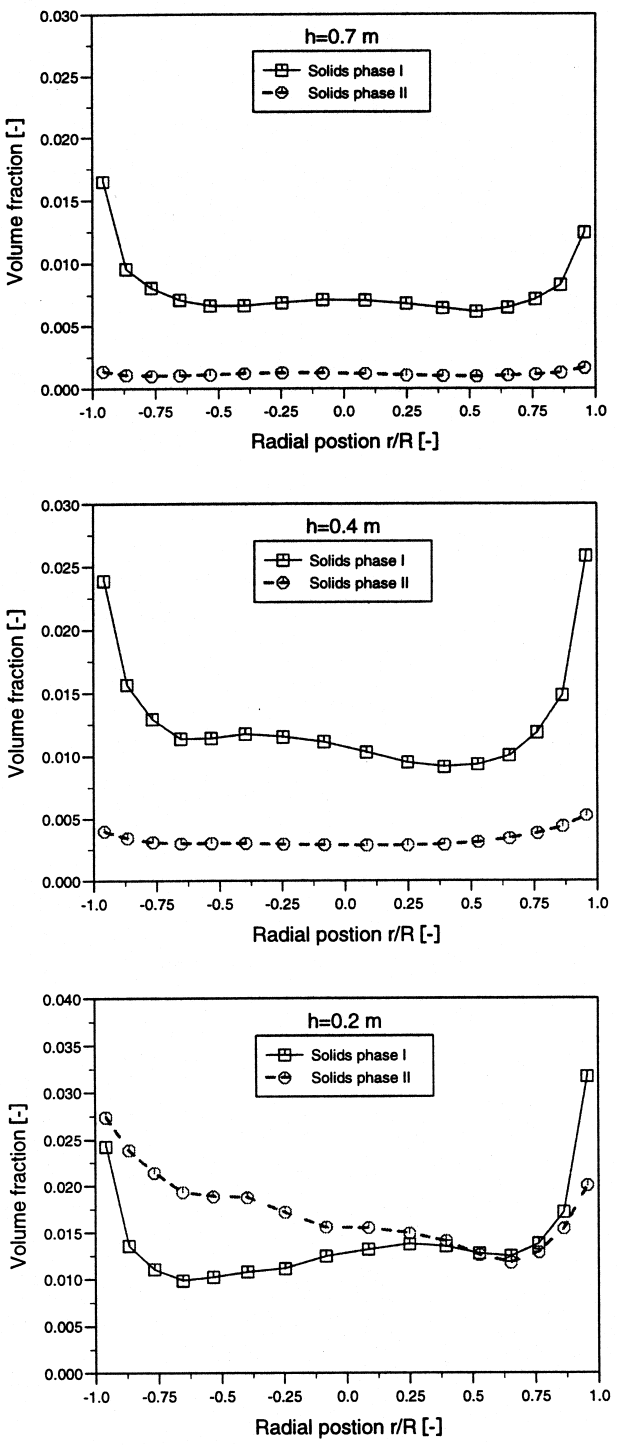

Fig. 8. Computed volume fraction profiles, $V_{SUP} = 1.0$ m/s.

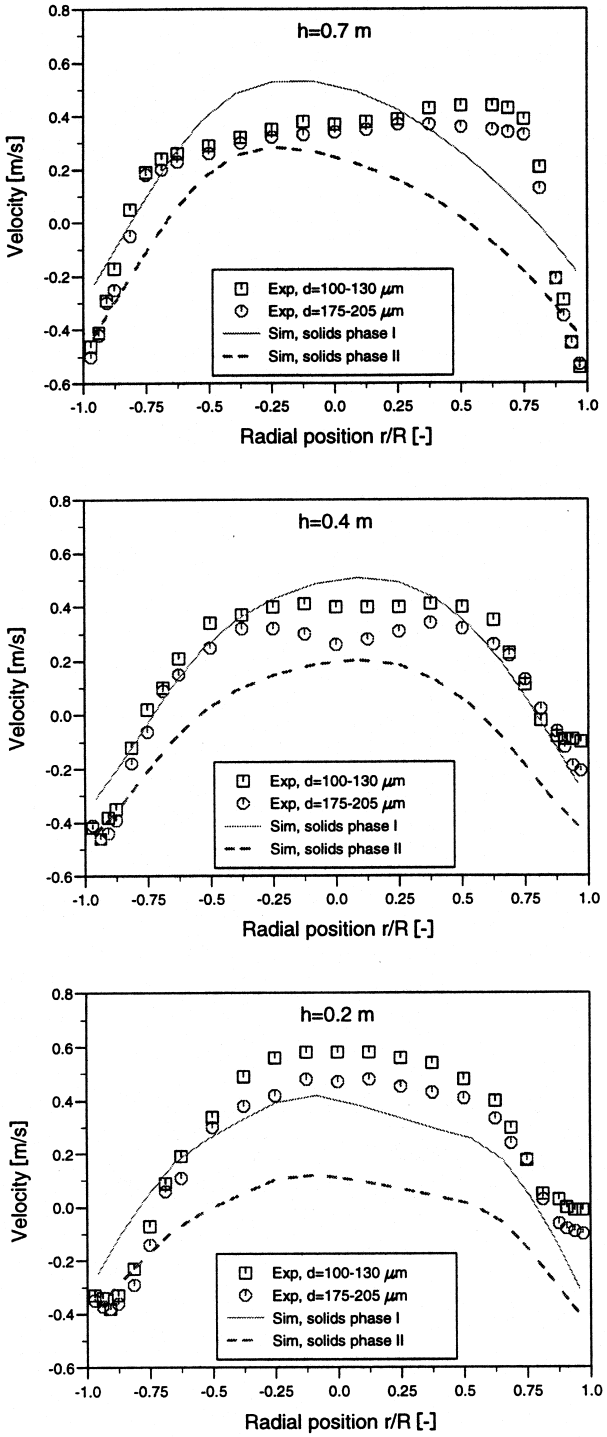

Fig. 9. Particle velocity profiles at different heights, $V_{SUP} = 1.0$ m/s.

wall region where the gas velocity is very low. Another important factor in a circulating fluidized bed will be that the smallest particle will probably circulate in the whole system, up in the core region and recirculate back through the standpipe. Larger particles will also start flowing up in the core, and then loose the momentum and start falling down near the wall. Thus, a larger mean diameter is observed in the annulus than in the core region.

In CFD modeling of bubbly two-phase flow, Lahey (1995) and others have shown that a transverse force has significant influence on the radial phase distribution. The transverse force is proportional to the axial velocity gradient in radial direction of the continuous phase and the relative velocity between the dispersed and continuous phase. It may be reasonable that this force should have an influence also in a gas/solid flow system. To test this, the transverse force was included into the mathematical model. However, the simulations show that the transverse force in a gas/solid flow system has only small effects on the flow pattern.

A Magnus-type force which is produced by spin and rotation of particles may have effects on the radial segregation. This force is more complex to implement in the model and is not included, but the effects should be studied in the future.

7.2. Volume fraction profiles

The LDA/PDA system delivered by DANTEC is only able to estimate the concentration of solid by the Time Ratio Technique. The technique has the limitations that there should be only one particle in the measuring volume at the same time and that this particle is less than the measuring volume. Since the width of the measuring volume is 150 μm and the system cannot be characterized as very dilute, there may be significant errors in the volume fractions measurements. However, the volume fraction measurements should give a good indication of the order of magnitude and general trends.

Fig. 7 shows the measured and computed radial volume fraction profiles of solid at three different heights for a superficial gas velocity of 1.0 m/s. The general agreement between the experimental and numerical results is fairly good. The simulated and measured profiles have the same form. At all heights the solid concentration distribution are as expected, dilute in the core region and more dense in the wall region in the simulation as well as in the measurements. The solid concentration is most dense at height 0.2 m. The heights 0.4 and 0.7 m seem to be in the freeboard zone, and the solid concentration is more dilute. At these two heights there are larger differences between the concentration of solid in the annulus and in the core regions.

The computed volume fraction profiles of each solid phase are shown in Fig. 8. For both phases, the concentration of solid increases from the center of the riser and toward the wall. Similar to the mean diameter, the radial concentration gradient seems to increase with height above the inlet. The smallest particles (solid phase I) separate more distinctly between the annulus and the core regions than the larger ones (solid phase II). The largest particles have not the same increase of the volume fraction in the wall region, as the smaller solid.

7.3. Particle velocity profiles

Measured and computed particle velocity profiles for each particle group are presented in

Fig. 9. The particle velocity profiles are obtained with a superficial gas velocity of 1.0 m/s, and 0.2, 0.4 and 0.7 m above the main gas inlet.

As illustrated in the figure, the particles move upward in the central part of the riser and downward near the walls, a behavior which is typical for core-annulus flow. The behavior is clearly observed in the experiments as well as in the simulations. At all heights, the negative velocities in the wall regions are almost correctly predicted. The computed core velocities are in good agreement with the experimental results, although a too low velocity is obtained at height 0.2 m above the primary gas inlet.

The measured velocity profiles show a relative velocity between particles of different sizes in the core region. In the wall region, no significant velocity deviation is observed in the experiments. The relative velocities are expected and caused by different gas-particle drag, for different particle sizes. The particle–particle drag, which is a strong function of the particle collisions will also play a major role at the magnitude of the relative velocity. The particle–particle drag decreases normally in a dilute gas/solid system where the particle–particle collisions are of less importance. The relative velocity decreases slightly with the height above the gas inlet, due to a lower mean velocity in the upper part of the riser.

The simulation shows a behavior similar to the measurements even though the relative velocity is a little too high at all heights, probably due to a too small estimated particle–particle drag. A too large computed relative particle velocity may be one of the reasons for the incorrectly obtained mean diameters in the annulus region. A too low particle velocity of the largest particle will give a too low circulation of larger particles in the riser and, hence, an incorrect radial diameter distribution.

Figs. 10 and 11 show the velocity profiles at height 0.4 m obtained with superficial gas velocity of 0.8 and 1.2 m/s, respectively. The same trends are observed, typical core-annulus flow and a relative velocity between the particles of different sizes in the central part of the riser. The relative velocity increases slightly with the superficial gas velocity. The simulations

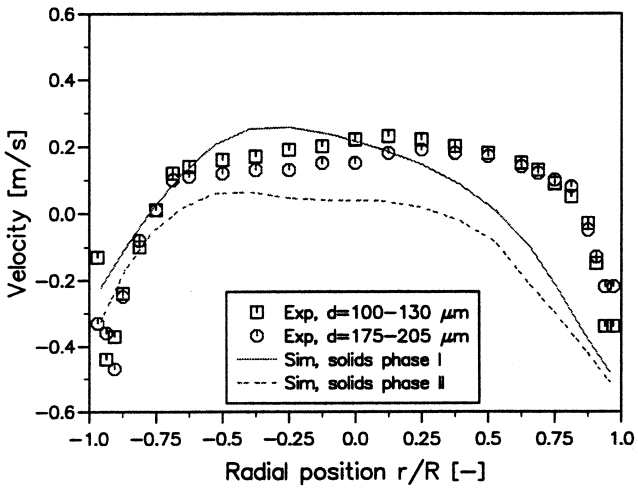

Fig. 10. Particle velocity profiles, $h = 0.4$ m and $V_{SUP} = 0.8$ m/s.

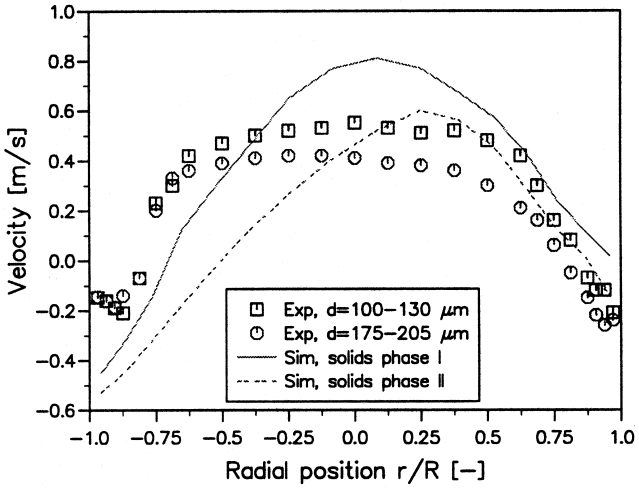

Fig. 11. Particle velocity profiles, $h = 0.4$ m and $V_{SUP} = 1.2$ m/s.

are in a fairly good agreement with the measurements, and a typical core-annulus flow with a relative velocity between the solid phases are obtained for all flow conditions.

7.4. Fluctuating particle velocity

A comparison of the experimental and numerical results is done in Fig. 12. The particle RMS velocity profiles are obtained at heights 0.2, 0.4 and 0.7 m and with a superficial gas velocity of 1.0 m/s.

The computed particle RMS velocities are derived from the definition of granular temperature:

$$V_{RMS} = \sqrt{3\theta_s} \tag{48}$$

The RMS velocities from experiments are found by Eq. (4). The RMS velocity profiles are measured for each particle group, and calculated for each solid phase.

For a very dilute gas/solid flow system that is considered in these experiments, the fluctuating velocity or the turbulence is mainly produced by shear. The RMS velocity in such a system increases from the center of the riser toward the wall. The turbulence decreases slightly with the height of the riser. At height 0.2 m, where the concentration of solid is more dense, particle–particle collisions have significantly influence the magnitude of the turbulence. Hence, the turbulence does not increase as much in the shear layer at this height, as at 0.4 and 0.7 m, where the concentration of solid is more dilute.

The general trends in the simulation are in a relatively good agreement with the experimental results. However, the simulations are a little too low at the heights 0.2 and 0.4 m. The relative particle RMS velocity decreases correctly with the height of the riser, and a small increase of the turbulence in the shear layer is obtained in the simulation. The model calculate correctly the highest turbulence for the smallest particles (solid phase I).

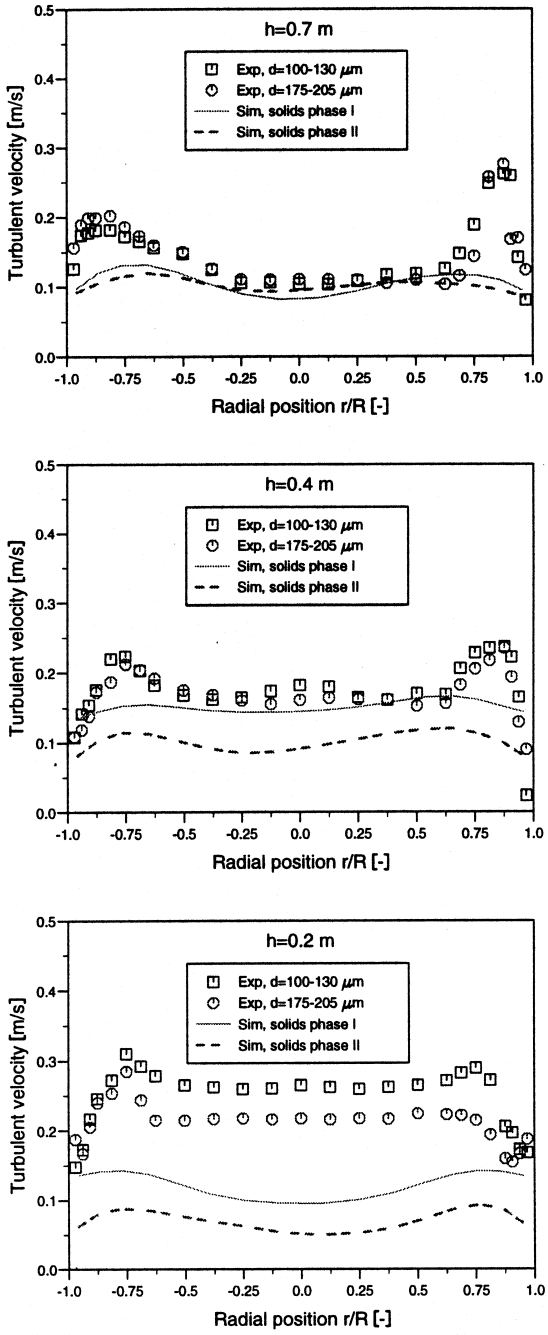

Fig. 12. Particle RMS velocity profiles at different heights, $V_{SUP} = 1.0$ m/s.

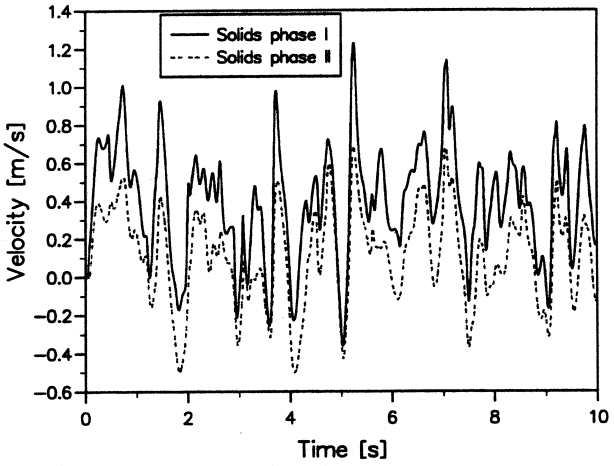

Fig. 13. Large scale velocity fluctuations, $h = 0.2$ m, $V_{SUP} = 1.0$ m/s.

A gas/solid flow system, like a circulating fluidized bed, will never reach a normal steady state condition. The system will exhibit a fluctuating behavior. In modeling such systems, the kinetic theory for granular flow takes care of the small scale fluctuations which are present. The large scale fluctuations are also simulated. Figs. 13 and 14 show the calculated large scale velocity fluctuations for each solid phase at the center line, 0.2 and 0.7 m above the gas inlet, respectively. The fluctuations are plotted for the first 10 s of real time and with a superficial gas velocity of 1.0 m/s. The large scale velocity fluctuations have the same frequency, and the relative velocity between the solid phases is nearly constant. A wide range of particle velocities is observed, including positive and negative velocities. In the experiments, the large scale fluctuations were easy to observe visually.

The large scale fluctuating flow behavior of a circulating fluidized bed will obviously also

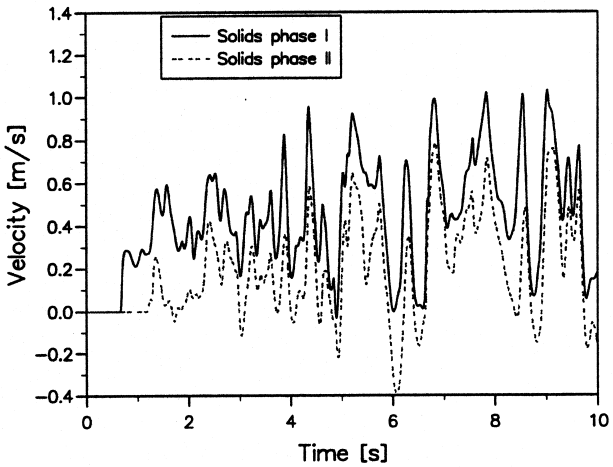

Fig. 14. Large scale velocity fluctuations, $h = 0.7$ m, $V_{SUP} = 1.0$ m/s.

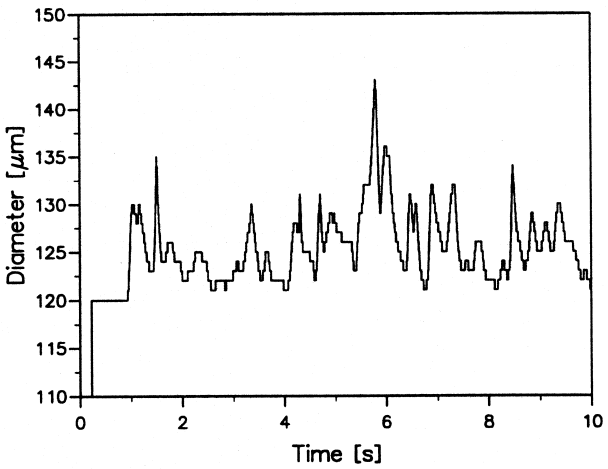

Fig. 15. Diameter fluctuations, $h = 0.4$ m, $V_{SUP} = 1.0$ m/s.

lead to a fluctuating mean diameter. The computed fluctuating diameter at the centerline, 0.4 m above the gas inlet is shown in Fig. 15. The frequency of the diameter fluctuations have the same order of magnitude as the velocity fluctuations. The number averaged diameter fluctuates between 120 and 145 μm.

The large scale velocity fluctuations as well as the small scale fluctuations are included in the measurements of the particle RMS velocity profiles. Hence, the computed RMS velocity from the granular temperature cannot be compared directly with the measured RMS velocity. The computed large scale fluctuations give rise to an extra RMS velocity which is added to the RMS velocity from the granular temperatures. The total RMS velocity is compared against the experimental data in Fig. 16. Although the large scale fluctuations seem to be significant, they have only minor effects on the total particle RMS velocity of each phase. The large scale velocity fluctuations are highest and have most influence on the total RMS velocity in the shear layers.

8. Concluding remarks

An extensive experimental study of the flow behavior of group B particles in a cold flow laboratory scale circulating fluidized bed using LDA and PDA is performed. Mean and RMS particle velocities are obtained for two different particle sizes. In addition, solid volume fraction and mean diameter are measured. The experimental results are analyzed and may be summarized as follow:

- A typical core-annulus flow behavior is observed in the riser.
- A relative particle velocity between small and larger particles is measured. The relative velocity is largest in the center of the riser and decreases toward the walls.
- The turbulent velocity is almost constant in the center of the riser and increases in the shear layer.

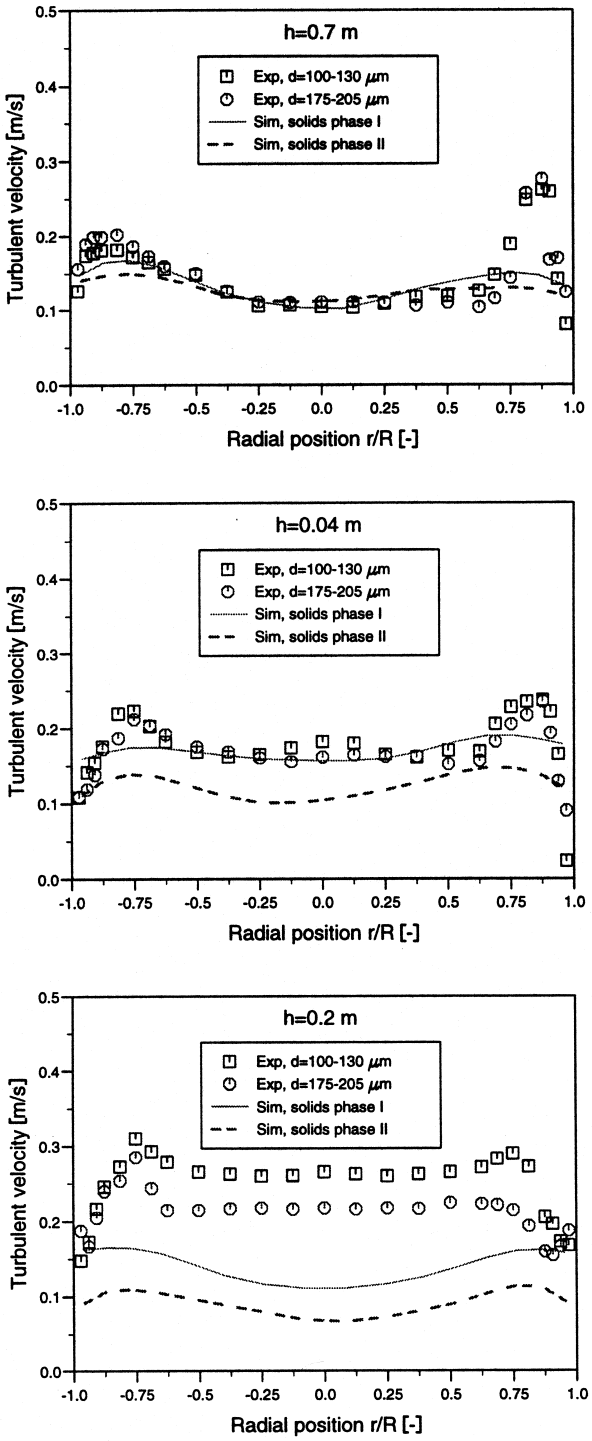

Fig. 16. RMS velocity profiles added large scale fluctuations, $V_{SUP} = 1.0$ m/s.

- A relative particle RMS velocity is observed in the lower part of the riser. Smaller particles fluctuate more than larger ones. In the upper part of the riser, the turbulent velocity seems to be nearly independent of the particle size.
- The solid concentration is dilute in the core region and denser in the annulus zone.
- An axial segregation by size is shown. The axial segregation decreases when the superficial gas velocity increases.
- A significant radial segregation of the mean diameter is shown, a behavior which seems not to be observed or reported in earlier studies of fluidized beds.

A three-dimensional Computational Fluid Dynamics (CFD) model has been developed based on earlier works at Telemark Technological R and D Centre (Tel-Tek). The model is based on an Eulerian description of the phases where the kinetic theory for granular flow forms the basis for the turbulence modeling in the solid phases. The model is generalized for one gas phase and N number of solid phase to enable a realistic description of particle size distributions and a non-uniform diameter distribution in gas/solid systems. Each solid phase is characterized by a diameter, form factor, density and restitution coefficient. The granular temperature and momentum equations are solved for each phase.

The circulating fluidized bed loop is simulated using a 2D Cartesian coordinate system. Two solid phases are used to describe two distinct particle groups. The simulations are in a fairly good agreement with the measurements. The core-annulus flow is correctly computed and the solid concentration seems to be relatively well predicted. However, the relative velocity between the solid phases is somewhat overpredicted. This may be due to the underestimated turbulent kinetic energy in the lower part of the riser, since the particle–particle drag is proportional to the square root of the granular temperature. In the upper part of the riser, the computed turbulence has a correct form and magnitude, although the turbulence in the shear layer is somewhat too low.

For different superficial gas velocities, the mathematical model is capable of estimating the axial segregation by size very well. But the model is not able to predict the significant radial variation of the mean diameter. The underestimation of the turbulence in the lower part may be a reason for the discrepancy between measured and simulated mean diameter in the wall region. The radial segregation may also be a result of external forces which are not included in the mathematical model.

The large scale fluctuations which occur in a gas/solid flow system are calculated and added to the small scale fluctuations obtained by the granular temperature. Although the large scale fluctuations seemed significant, they increased the total particle RMS velocity very little. The model correctly calculate the higher level of turbulence, for the largest particles.

Acknowledgements

The authors would like to express their thanks to Norsk Hydro, Statoil and The Research Council of Norway (NFR) for their financial support of this work.

References

Bachalo, W.D., Houser, M.J., 1984. Phase Doppler spray analyzer for simultaneous measurements of drop size and velocity distributions. Opt. Engineering 25 (5), 583–590.

Bagnold, R.A., 1954. Experiments on a gravity-free dispersion of large solid spheres in a Newtonian fluid under shear. Proc. Roe. Soc A255, 49–63.

Boemer, A., 1996. Consistency of the granular multiphase model, private communication.

Deardorff, J.W., 1971. On the magnitude of the subgrid scale eddy coefficient. J. Comp. Phys 7, 120–133.

Ding, J., Gidaspow, D., 1990. Bubbling fluidization model using kinetic theory of granular flow. AIChE J 36 (4), 523–538.

Durst, F., Zare, M., 1975. Laser-Doppler measurements in two-phase flows. In: Proceedings of the LDA-Symposium, Copenhagen, pp. 403–429.

Enwald, H., Peirano, E., Almstedt, A.-E., 1996. Eulerian two-phase flow theory applied to fluidization. Int. J. Multiphase Flow 22 Supplement, 21–66.

Ergun, S., 1952. Fluid flow through packed columns. Chem. Eng. Prog 48, 89–94.

Geldart, D., 1973. Types of gas fluidization. Powder Technology 7, 285–295.

Gidaspow, D., 1994. Multiphase Flow and Fluidization. Academic Press, Boston.

Gidaspow, D., Huilin, L., Manger, E., 1996. Kinetic theory of multiphase flow and fluidization: validation and extension to binary mixtures. In: Nineteenth Int. Cong. of Theoretical and Appl. Mech., August, Kyoto, Japan, pp. 25–31.

Hjertager, B.H., 1997. Computational fluid dynamics (CFD) analysis of multiphase chemical reactors. Delft University of Technology, 25–29 August. Also 1998, Trends in Chem. Eng. 4, 45–92.

Jenkins, J.T., Mancini, F., 1987. Balance laws and constitutive relations for plane flows of a dense binary mixture of smooth, nearly elastic circular disks. J. Appl. Mech 54, 27–34.

Jenkins, J.T., Savage, S.B., 1983. A theory for the rapid flow of identical, smooth, nearly elastic, spherical particles. J. Fluid Mech 30, 187–202.

Lahey, R.T., 1995. CFD modelling of phase distribution and separation phenomena: Part 17B. Multiphase Flow and Heat Transfer, Computational Modelling. Swiss Federal Institute of Technology, March 20–24, Zurich, Switzerland.

Lebowitz, J.L., 1964. Exact solution of generalized Percus–Yevick equation for a mixture of hard spheres. The Physical Review 133 (4A), 895–899.

Lun, C.K.K., Savage, S.B., Jeffrey, D.J., Chepurniy, N., 1984. Kinetic theories for granular flow: inelastic particles in couette flow and slightly inelastic particles in a general flowfield. J. Fluid Mech 140, 223–256.

Manger, E., 1996. Modelling and simulation of gas/solid flow in curvilinear coordinates. Ph.D. thesis, Telemark Institute of Technology, Norway.

Mathiesen, V., Solberg, T., Manger, E., Hjertager, 1996. Modelling and predictions of multiphase flow in a pilots-cale circulating fluidized bed. Proc. 5th Int. Conf. on Circulating Fluidized Beds, May 28–31, Beijing, China.

Patankar, S.V., 1980. Numerical Heat Transfer and Fluid Flow. Hemisphere, Washington DC.

Rowe, P.N., 1961. Drag forces in a hydraulic model of a fluidized bed, Part II. Trans. Inst. Chem 39, 175–180.

Saffmann, M., Buchhave, P., Tanger, H., 1984. Simultaneous measurements of size concentration and velocity of spherical particles by a laser doppler method. In: Adrian, R.J., Durano, D.F.G., Durst, F., Mishina, H., Whitelaw, J.H. (Eds.), Laser Anemometry in Fluid Mechanics—Part II. Ladoan Instituoto Superior Tecnico, Lisboa, Portugal.

Samuelsberg, A., Hjertager, B.H., 1996a. An experimental and numerical study of flow patterns in a circulating fluidized bed reactor. Int. J. Multiphase Flow 22 (3), 575–591.

Samuelsberg, A., Hjertager, B.H., 1996b. Computational modelling of gas particle flow in a riser. AIChE J 42 (6), 1536–1546.

Sekoguchi, K., Takeishi, M., Kano, H., Hironaga, K., Nishiura, T., 1982. In: First Int. Symp. on Appl. of Laser Anemometry to Fluid Mech. Paper 16.1, Lisboa, Portugal.

Spalding, D.B., 1983. Developments in the IPSA procedure for numerical computation of multiphase-flow phenomena with interphase slip, unequal temperatures, etc. In: Numerical Properties and Methodologies in Heat Transfer. Hemisphere, Washington DC, pp. 421–476.

Spalding, D.B., 1985. Computer simulation of two-phase flows with special reference to nuclear reactor systems. In: Lewis, R.W., Morgan, K., Johnson, J.A., Smith, W.R. (Eds.), Computational Techniques in Heat Transfer. Pineridge, Swansea, p. 44.

Wen, C.Y., Yu, Y.H., 1966. Mechanics of fluidization. Chem. Eng. Prog. Symp. Series 62, 100–111.

Yakhot, Y., Orszag, S.A., 1986. Renormalization group analysis of turbulence. Part 1: basic theory. J. Scientific Computing 1 (1), 3–51.

Zamankhan, P., 1995. Kinetic theory of multicomponent dense mixtures of slightly inelastic spherical particles. Phys. Rev. E 52 (5), 4877–4891.